Journal of Materials Chemistry B

Accepted Manuscript

This is an *Accepted Manuscript*, which has been through the Royal Society of Chemistry peer review process and has been accepted for publication.

Accepted Manuscripts are published online shortly after acceptance, before technical editing, formatting and proof reading. Using this free service, authors can make their results available to the community, in citable form, before we publish the edited article. We will replace this *Accepted Manuscript* with the edited and formatted *Advance Article* as soon as it is available.

You can find more information about *Accepted Manuscripts* in the Information for Authors.

Please note that technical editing may introduce minor changes to the text and/or graphics, which may alter content. The journal's standard Terms & Conditions and the Ethical guidelines still apply. In no event shall the Royal Society of Chemistry be held responsible for any errors or omissions in this *Accepted Manuscript* or any consequences arising from the use of any information it contains.

ROYAL SOCIETY OF CHEMISTRY

www.rsc.org/materialsB

Redox Responsive Pd (II) Templated Rotaxane Nanovalve Capped Mesoporous Silica Nanoparticles: A Folic Acid Mediated Biocompatible Cancer-targeted Drug Delivery System

Srivardhan Reddy Gayam, Shu–Pao Wu*

Department of Applied Chemistry, National Chiao Tung University, Hsinchu, 30010, Taiwan, Republic of China

*Corresponding author at: 1001 Ta Hsueh Road, Hsinchu, 30010, Taiwan, Republic of China

Tel.: +886-3-5712121 ext 56501; fax: +886-3-5723764.

E–mail: spwu@mail.nctu.edu.tw (S. Wu)

Journal of Materials Chemistry B Accepted Manuscript

Abstract

In this study, we report a redox responsive drug delivering nanocarrier design, based on mesoporous silica nanoparticles. Gatekeeping of the mesopore is achieved by Pd(II) templated, mechanically interlocked rotaxane nanovalves with a folic acid terminal group, anchored by a disulfide bridge as a snap-top on the surface. The active metal templated rotaxane approach helps in quick and irreversible gate formation for effective utilization of the drug. The folic acid head group bestows targeting capability, specifically to cancer cells. Once nanoparticles enter the cancer cell, controlled release of the cargo is triggered by cleavage of the disulfide bond using an endogenous glutathione stimulus. In addition to having efficient drug loading and controlled release mechanisms, this smart biocompatible carrier system showed obvious uptake and consequent release of the drug in HeLa cells, demonstrating its use as a potential theranostic material.

Keywords: controlled release; drug delivery; mesoporous silica nanoparticles;redox.

Journal of Materials Chemistry B Accepted Manuscript

1. Introduction

In the last few decades, advances in modern biology have helped design and develop pharmaceutical drugs with numerous effective therapeutic strategies.[1] However, the current treatment methods for cancer are primarily dependent on the use of conventional cytotoxic drugs, which affect the normal, fast-growing cells, potentially damaging the vital organs.[2] Many studies have suggested that these problems could be attributed to the lack of target specificity of the conventional chemotherapeutic drugs.[3] To overcome this impediment, biocompatible target-specific drug delivery systems have to be designed in order to deliver an effective dosage of drug molecules and various other therapeutic agents, to the affected organs and cells, while sparing normal tissues.

Breakthroughs in nanobiotechnology have received great attention, owing to the potential of nano transporting systems, which have long been scaled to the nanometer size range. Mesoporous silica nanoparticles (MSNP) are promising materials that act as a multifunctional transport platform capable of delivering therapeutic elements to a variety of disease models at cellular and in vivo levels.[4,5] The main advantages of using MSNPs are the uniform monodisperse particle size (ranging from 50 to 200 nm), high surface area (800 – 1200 m^2 g^{-1}), morphology,[6,7] easy surface chemical modification[8-10] and porosity, along with their chemical stability and biocompatibility.[11-13] The use of MSNPs as a drug delivery system was reported for the first time in 2001,[11] 9 years after the discovery of the MCM-41 family by Mobil Corporation in 1992.[6] Since then, promising biomedical applications of MSNPs as multifunctional transport platforms are being developed to deliver therapeutic elements to target cells and tissues upon exposure to a predetermined pH,[14,15] redox potential,[16-18] photo response,[19,20] reactive oxygen species[21] and enzyme

Journal of Materials Chemistry B Accepted Manuscript

activity[22,23] as stimuli. The stimuli responsive drug delivery systems (SRDDS) are potentially useful theranostic agents for disease therapy and also aid in monitoring biodistribution, cancer cell targeting efficiency, internalization pathways,[24,25] cytotoxicity and progress of therapy.[26,27]

Cancer is one of the major causes of death among all diseases affecting humans.[28] It is evident that there is a need for design and development of effective therapeutic strategies to address it. Extensive research by biologists to understand physiological differences between normal and cancer cells has allowed the design of an effective, target-specific SRDDS for cancer therapy. It is well known that cancer cells generally overexpress folate receptors (compared to normal cells) due to a high metabolic demand for rapid proliferation. Similarly, it is well understood that glutathione (GSH), which is abundant in cancer cells, plays a very crucial role in cancer metabolism. Hence folate functionalized, MSNPs based SRDDS can effectively target cancer cells while endogenous GSH could be used as a trigger to initiate drug release.[29-32]

Careful choice of a gating mechanism in such SRDDS is necessary as they play an important role in holding the cargo and its delivery. Rotaxane nanovalves have previously been used as gatekeepers for MSNPs in which the macrocycle molecule (cyclodextrins, cucurbit[6]uril, crown ethers) encircles the stalk at the recognition site *via* non-covalent interactions.[33-35] However, in our work we used an active metal template rotaxanation approach for capping of mesopore in which the macrocycle molecule encircles the stalk via coordination-covalent interactions. This binding interactions influence several physicochemical properties such as rotaxanation kinetics, stability, and yield. In general, rotaxanation kinetics, stability, and yield are higher for active metal template rotaxanation approach than rotaxanation via non-covalent

Journal of Materials Chemistry B Accepted Manuscript

interactions. These beneficial parameters for active metal template rotaxanation approach promote the efficient and quick capping of mesopore, what helps the effective utilization of the drug. Since the discovery of the metal templating rotaxination approach by Sauvage et al,[36] the modular synthetic strategy prompted scientists to design fascinating interlocked molecules. However, till date, metal templated [2]rotaxane has not been utilized in devising a mechanized nanovalve. For the first time, we used this approach to design a rotaxane nanovalve as a gatekeeper for MSNP, in which the macrocycle molecule (macrocycle Pd-tridentate ligand) encircles the stalk through the coordination bond (but not by weak forces). Using this strategy, effective utilization of expensive drugs is made possible than other rotaxanes form via supramolecular interactions by enhancing the yield of rotaxination with immediate and more stable (irreversible) capping of mesopores. In general, metal ions have an important role in biology and medicine. Metal chelated macromolecular conjugates have also been used as potential pharmaceutical agents.[37,38] In addition to aiding macromolecular assembly, we believe that the metal templated approach with further development of the rotaxane nanovalves can potentially be used as a theranostic agent. Keeping in mind all necessary qualities for an ideal drug delivery system, we carefully designed a redox responsive controlled drug delivery system with a folic acid head group in the [2]rotaxane unit as a snap-top to address the site specific drug release as illustrated in Figure 1. Nanoparticles loaded with the anticancer drug doxorubicin (Dox) were evaluated as a drug-release system in HeLa cell cultures and their effect on the apoptosis mechanism of the cells was studied with the MTT cell viability assay and confocal laser scanning microscopy.

2. Experimental

2.1 Materials

Journal of Materials Chemistry B Accepted Manuscript

Absolute ethanol (EtOH, > 99.9%), acetonitrile were purchased from C-ECHO. Acetic acid, 2-aminoethythiol hydrochloride, 3-aminopropyltriethoxysilane (APTS), cetyltrimethylammonoium bromide (CTAB, 90%), 4', 6-diamidino-2-phenylindole (DAPI), 3-mercaptopyltrimethoxysilane (MPTMS), and tetraethylorthosilicate (TEOS, 99%) were purchased from Alfa Aesar. 3-(4,5-Dimethylthiazol-2-yl)-2,5-diphenyltetrazolium bromide (MTT), 2,2'-dithiodipyridine, dithiothreitol (DTT), doxorubicin (Dox), dulbecco's modified eagle's medium (DMEM), fluorescein, glutathione (GSH), 10% Pd/C catalyst, and sodium azide (NaN_3) were purchased from Sigma–Aldrich. Magnesium sulfate ($MgSO_4$) was purchased from Showa. Hydrochloride (HCl, assay 37%), potassium carbonate (K_2CO_3), and sodium hydroxide (NaOH) were purchased from Union Chemical Works (UCW). Diethyl ether, dimethylformamide (DMF, 99%), methanol (MeOH, 99.5%), and tetrahydrofuran (THF) were purchased from Aencore. All the solvents were HPLC grade; anhydrous solvents were obtained by standard distillation drying procedures and further dried by treated with activated silica. Solvents were degassed by freeze/thaw/pump cycle technique prior to use. Thin layer chromatographies (TLC) were performed on TLC silica gel 60 F_{254} (Merck). The plates were visualized using ultraviolet light (256 nm). Flash chromatographies were performed on Merck silica gel 60 (230-400 mesh) under pressure using desired solvents.

2.2 Instruments

NMR spectra were recorded on Bruker DRX-300 NMR spectrometer. Chemical shifts were reported in parts per million (ppm) from low to high field and referenced to residual solvent ($CDCl_3$, δ = 7.26 ppm and δ = 77.23 ppm; DMSO-d_6, δ = 2.49 ppm and δ = 39.56 ppm respectively). Coupling constant (J) were reported in hertz (Hz). Standard abbreviations

Journal of Materials Chemistry B Accepted Manuscript

indicating multiplicity were used as follows: s = singlet, d = doublet, t = triplet, m = multiplet, br = broad. UV-Vis spectra were recorded using Agilent 8453 spectrophotometer. Fluorescence spectra were with HITACHI F-7000 fluorescence spectrophotometer. TEM images were recorded from JEOL JEM-2010 Transmission Electron Microscope. X-ray diffraction pattern was collected by low-angle Bruker D8 Discover XRD. Zeta potential was measured by Mavern Nanosizer. BET surface area and BHJ pore size distribution characterization were performed by Micromeritics ASAP 2020 Accelerated Surface Area and Porosimetry System. FT-IR spectra were collected through Bomem DA8.3 Fourier-Transform Infrared Spectrometer. Fluorescent images were taken on a Leica TCS-SP5-X AOBS Confocal Fluorescence Microscope.

2.3 Synthesis of compounds

The syntheses of S-(2-aminoethylthio)-2-thiopyridine hydrochloride, 3-(2-bromoethoxy)phenol, 3-(2-azidoethoxy)phenol, 3-(2-azidoethoxy)phenoxy)methyl)-6-(bromomethyl)pyridine, macrocyclic-Pd tridentate ligand, and alkyne-functionalized folic acid are described in the Supporting Information. They were characterized by ^{1}H NMR, ^{13}CNMR and MS.

Synthesis of MSNP–SH: Mesoporous silica nanoparticles were prepared by a conventional sol-gel process in base solution. Grafting method was used for the surface functionalization.[18] In a typical synthesis, CTAB (1 g) was dissolved in distilled H_2O (500 mL). NaOH aqueous solution (3.5 mL, 2M) was added into the above solution. The reaction mixture was stirred vigorously at 800 rpm at 80 ^{o}C. TEOS (5 mL) was slowly added into the mixture solution and the solution was stirred for 2 h. MSNPs were collected by centrifugation at 15000 rpm for 10 min, then washed with MeOH and Millipore DI water alternatively for several times until there was no trace of base (NaOH)

Journal of Materials Chemistry B Accepted Manuscript

left with MSNPs (it was monitored by pH litmus paper and pH meter). MSNPs were dried in vacuum at 80 °C for 24 h. The introduction of thiol units through grafting method was conducted by suspending as-prepared silica nanoparticles (500 mg) in MeOH (100 mL), followed by the addition of 3-mercaptopyltrimethoxysilane (MPTMS) (0.5 mL). The mixture was refluxed at 80 ^{o}C under N_2 atmosphere for 24 h. The thiol group functionalized silica nanoparticles were collected by centrifugation at 10000 rpm and washed with MeOH and DI water for 6 times. CTAB was removed by suspending the thiol group functionalized silica nanoparticles in MeOH (50 mL) containing HCl (3 mL) and refluxed for 24 h. MSNP–SH was collected by centrifugation 10000 rpm and washed thoroughly with MeOH and DI water until no HCl was left (it was monitored by pH litmus paper). MSNP–SH particles were dried in vacuum at 80 °C for 24 h.

Synthesis of MSNP–SS–NH_2: Disulfide bond formation was obtained by suspending MSNP–SH (300 mg) in MeOH (30 mL) followed by the addition of S-(2-aminoethylthio)-2-thiopyridine hydrochloride (200 mg). The mixture was stirred at room temperature for 24 h. MSNP–SS–NH_2 was collected by centrifugation, washed thoroughly with MeOH and DI water and dried under vacuum at 80 °C for 24 h. (Yield = 290 mg)

Synthesis of MSNP–SS–N_3: To the well suspended solution of MSNP–SS–NH_2 (200 mg) nanoparticles in acetonitrile (50 mL), K_2CO_3 (50 mg) was added. Then a solution of 2-(3-(2-azidoethoxy)phenoxy)methyl)-6-(bromomethyl)pyridine (200 mg) in acetonitrile (10 ml) was added slowly and stirred under reflux for 24 h. MSNP–SS–N_3 nanoparticles were collected by centrifugation at 10000 rpm, washed thoroughly with DI water until no K_2CO_3 was left. Then MSNP–SS–N_3 was washed with acetonitrile and

Journal of Materials Chemistry B Accepted Manuscript

MeOH alternatively for several times, and dried under vacuum at 80 °C for 24 h. (Yield = 187 mg).

Synthesis of macrocyclic-Pd tridentate ligand capped MSNP–SS–N_3: To a well suspended solution of MSNP–SS–N_3 nanoparticles (10 mg) in CH_2Cl_2/CH_3CN (10 mL, 8/2, V/V), fluorescein or Dox (3 mg) was added and stirred under dark conditions for 24 h. Fluorescein or Dox loaded nanoparticles were centrifuged, washed with dichloromethane (1 mL) for two times. Then the nanoparticles were suspended in a solution of macrocycle Pd-tridentate ligand (10 mg) in CH_2Cl_2/CH_3CN (10 mL, 8:2, V/V) and stirred for 12 hours. Fluorescein or Dox loaded nanoparticles were collected by centrifugation, washed with dichloromethane and dried.

Synthesis of MSNP–SS–FA: To a well suspended solution of macrocycle Pd-tridentate ligand capped MSNP–SS–N_3 nanoparticles (1 mg) in DMF/H_2O (1 mL, 8:2, V/V), alkyne-functionalized folic acid (1 mg) in DMF (100 μL), $CuSO_4.5H_2O$ (1 mg) in H_2O (20 μL) and sodium ascorbate (3 mg) in H_2O (20 μL) were added. The reaction mixture was stirred for 12 h, then washed with DI H_2O and dried.

2.4 Drug delivery test

The drug releasing experiments of the nanoparticles were conducted by adding 500 μL of as-prepared fluorescein loaded MSNP–SS–FA solution (1mg mL^{-1}, pH = 7.36) into PBS buffer (4.5 mL, pH = 7.36) with or without the reducing agent DTT or GSH (50 mM). The mixture (100 μL) was centrifuged at 13,000 rpm for 3 min, and the supernatant was monitored by fluorometer. Excitation wavelength was 492 nm and the emission wavelength at 515 nm was used for the fluorescein detection.

Journal of Materials Chemistry B Accepted Manuscript

2.5 MTT cytotoxicity assay

The cytotoxicity of the nanoparticles was evaluated by the MTT assay. MSNP–SS–FA, Dox-loaded MSNP–SS–FA and Dox samples were used in the cytotoxicity test. HeLa cells were grown into 96-well plate at a density of 1 × 104 cells/well in DMEM medium. After 24 h, the medium in the wells was replaced with fresh medium (200 μL) containing MSNP–SS–FA, Dox-loaded MSNP–SS–FA, equivalent amount of free Dox with different concentrations (10 to 125 μg). After incubation for another 24 h, 3-(4,5-dimethylthiazol-2-yl)-2,5-diphenyltetrazolium bromide (MTT) (20 μL, 0.5 mg mL^{-1}) was added. After further incubation for 4 h, the medium was removed, and DMSO (200 μL) and Sorenson's glycine buffer (0.1 M glycine and 0.1 M NaCl) were added. The plate was gently shaken for 15 min. Then, the absorbance at 570 nm was measured for each cell. The viability of cells was calculated according to the following equation: Cell viability (%) = (mean of absorbance value of treatment group) / (mean of absorbance value of control group)

2.6 Fluorescence microscopic images

HeLa cells were seeded in Ibidi standard bottomed μ-dishes (35 mm) and grown in the DMEM medium for 24 h. After HeLa cells were exposed to Dox loaded MSNP–SS–FA (50 μg mL^{-1}), and fluorescein loaded MSNP–SS–FA (50 μg mL^{-1}) for 2 h, the medium was removed and dishes were washed three times with PBS. DMEM medium was added with further 15 min incubation. HeLa cell images were taken by a Leica TCS-SP5-X AOBS Confocal Fluorescence Microscope.

Journal of Materials Chemistry B Accepted Manuscript

3. Results and Discussion

We synthesized MSNPs from tetraethyl orthosilicate (TEOS) using hexadecyltrimethylammonium bromide (CTAB) as a surfactant template agent. Thiol modification of nanoparticles (MSNP–SH) was achieved by surface grafting MSNPs with 3-mercaptopyltrimethoxysilane (MPTMS). Further, amino-terminated alkyl chains containing disulfide bond modified nanoparticles (MSNP–SS–NH_2) were obtained by the reaction with S-(2-aminoethylthio)-2-thiopyridine hydrochloride (Figure 2 and Scheme S1 in the supporting information). Construction of the stalk with an azide terminated, pyridine containing alkyl chain on the surface of MSNP–SS–NH_2 was achieved by the reaction with 3-(2-azidoethoxy)phenoxy)methyl)-6-(bromomethyl)pyridine to yield MSNP–SS–N_3. Desired cargo was loaded, after the stalk was encircled by the macrocycle Pd-tridentate ligand to form a rotaxane nanovalve. Finally, folic acid functionalized nanoparticles (MSNP–SS–FA) were obtained by using the copper(I) catalyzed click reaction. Thus, the rotaxane valves act as gatekeepers for the mesopore to lock the cargo molecules inside and the folic acid head group serves to specifically target cancer cells. Presence of the disulfide bond reducing agents such as glutathione (GSH) or dithiothreitol (DTT) can effectively open the rotaxane valve from the mesopore and lead to the release of the cargo molecules.

From dynamic light scattering (DLS) experiments and scanning electron microscopy (SEM) results, the average size of MSNP–SS–FA was estimated to be 100 ± 15 nm (see Figure S1 in the supporting information). A highly ordered mesoporous structure with hexagonal symmetry in nanoparticles was confirmed by HR-TEM and small angle powder X-ray diffraction (Figure 3 and Figure S2 in the supporting information).

Journal of Materials Chemistry B Accepted Manuscript

Interplanar distance measurements for 30 individual nanoparticles from the HR-TEM image reveal that the average interplanar spacing (d_{100}) of the mesopore is 3.4 nm. The interplanar distance of d_{100} planes in MSNP–SH, MSNP–SS–NH_2, and MSNP–SS–N_3 was calculated to be 3.48 nm by Bragg's law from the (100) position at $2\theta = 2.53°$, which is consistent with the value obtained from HR–TEM analysis. The mesoporous structure of MSNP–SS–FA was not observed in TEM analysis after capping with the macrocycle Pd-tridentate ligand (see Figure S4 in the supporting information). Surface areas of MSNP–SH, MSNP–SS–NH_2, MSNP–SS–N_3, and fluorescein loaded MSNP–SS–N_3, were studied by N_2 adsorption-desorption isotherms (see Figure S3 in the supporting information). A typical type-IV isotherm pattern was observed in MSNP–SH, MSNP–SS–NH_2, and MSNP–SS–N_3 with a Brunauer–Emmett–Teller (BET) surface area of 1096 $m^2\ mL^{-1}$, 1077 $m^2\ mL^{-1}$ and 865 $m^2\ mL^{-1}$ respectively. The pore size of 2.6 nm was obtained by Barrett-Joyner-Halenda (BJH) desorption, indicating a highly ordered mesoporous structure of nanoparticles. Fluorescein loaded MSNP–SS–N_3 showed a type-II isotherm with low BET surface area, 317 $m^2\ mL^{-1}$ due to the pore of the mesopore filling with fluorescein, indicating efficient loading of fluorescein in mesopores (Figure S3). The thickness of the mesopore wall was estimated to be 0.9 nm, from the difference between the lattice interplanar distance calculated using XRD (3.48 nm) and the internal average pore size given by the BJH method (2.6 nm).

Each functionalization step on MSNPs was fully characterized using FT–IR analysis and zeta potential measurements. As seen from the FT–IR spectra (Figure 4), the complete removal of surfactant from mesoporous silica was validated by the disappearance of the typical alkyl C–H stretching frequencies at 2850 cm^{-1} and 2922 cm^{-1}

Journal of Materials Chemistry B Accepted Manuscript

of the surfactant CTAB (from Line a to b in Figure 4). Successful grafting of MPTMS to introduce thiol groups on MSNP was confirmed by the appearance of the thiol S–H stretching frequency at 2570 cm^{-1} (Figure 4B). Functionalization of MSPN–SH to MSNP–SS–NH_2 was verified by the appearance of the typical amine N–H bending frequencies at 1571 cm^{-1} (Figure 4C) and the disappearance of the S–H stretching frequency at 2570 cm^{-1} (Figure 4B). Further modification of MSNP–SS–NH_2 to MSNP–SS–N_3 was validated by the appearance of the characteristic strong azide N=N=N stretching frequency at 2107 cm^{-1} (from Line c to d in Figure 4). The final functionalization of MSNP–SS–N_3 to MSNP–SS–FA was verified by the disappearance of the strong azide N=N=N stretching frequency at 2107 cm^{-1} and the presence of the typical strong carbonyl (C=O) stretching frequencies at 1658 cm^{-1} (from Line d to e in Figure 4). These results indicate the successful functionalization of mesoporous silica nanoparticles with a disulfide bond linker and terminal folic acid.

Successful functionalization of MSNPs with the folic acid and disulfide bond–bridged functional group on MSNP–SS–FA was further confirmed by zeta potential measurements (see Figure S5 in the supporting information). The modification of MSNPs to MSNP–SH was confirmed by the change in zeta potential from −41.73 mV to −28.43 mV on account of the modification of negative Si–OH groups on the surface of MSNPs by relatively less negatively charged −SH groups. After the formation of MSNP–SS–NH_2 from MSNP–SH, the surface charge was turned into a highly positive value of +33.9 mV, due to the positively charged –NH_3^+ units on the surface. Further modification of MSNP–SS–NH_2 to MSNP–SS–N_3 was validated by the change in zeta potential from a positive value (+33.9 mV) to a negative value (−4.98 mV) due to the azide (–N_3) units on the

Journal of Materials Chemistry B Accepted Manuscript

surface. The final functionalization of MSNP–SS–N_3 to MSNP–SS–FA was confirmed by the increase in zeta potential from –4.98 mV to + 41.62 mV due to the presence of a positively charged Pd metal center and $–NH_2$ units of the folic acid on the surface. This was further confirmed by the XPS analysis where the orbital bands of Pd, $^3d_{5/2}$ and $^3d_{3/2}$ were observed at 336 and 342 eV, respectively (see Figure S6 in the supporting information).[39] The surface density of rotaxane nanovalves integrated on MSNPs was estimated to be approximately 66 mg g^{-1} by thermogravimetric analysis (see Figure S7 in the supporting information).

In order to measure the drug delivery capacity of MSNP–SS–FA, nanoparticles were loaded with either fluorescein or Dox in PBS buffer with a weight ratio of 10:3 (nanoparticle: fluorescein or Dox) at room temperature for 24 h. The fluorescein loading capacity of MSNP–SS–FA was calculated to be around 14 ~ 17 μg per 1 mg of nanoparticles (see Figure S8 in the supporting information) and 11 ~ 13 μg per 1 mg of nanoparticles for doxorubicin. The controlled drug delivery of MSNP–SS–FA was investigated by monitoring the fluorescent intensity changes of fluorescein loaded nanoparticles in PBS buffer (pH = 7.4). Without the addition of any reducing agent, fluorescein loaded MSNP–SS–FA did not exhibit obvious cargo leakage (Figure 5), indicating that the rotaxane snap top nanovalves on the surface can block fluorescein release from the mesopores. With the introduction of reducing agents DTT or GHS, obvious fluorescein releases were observed.

The anticancer drug doxorubicin (Dox) was employed to investigate the cytotoxicity and delivery capacity of the functional nanoparticles. The MSNP–SS–FA nanoparticles have no considerable cytotoxicity towards HeLa cells, according to the MTT assay. The cell viability has

Journal of Materials Chemistry B Accepted Manuscript

shown no significant decrease with increasing nanoparticle concentrations. Relatively high cell viabilities (about 80%) were observed even at a high nanoparticle concentration of 130 μg mL^{-1}, indicating that the MSNP–SS–FA nanoparticles are biocompatible (Figure 6). Cell viability for free Dox has shown relatively less cytotoxicity towards HeLa cells, compared to the Dox-loaded MSNP–SS–FA. Cell viability has clearly shown a significant decrease with increasing Dox-loaded MSNP–SS–FA nanoparticle concentration. Relatively very less cell viabilities (about 30%) (Figure 6) were observed at a high nanoparticle concentration of 130 μg, demonstrating that the MSNP–SS–FA is an effective, stimuli responsive cancer targeted drug delivery system.

In order to understand how well the prepared MSNP–SS–FA nanoparticles can be endocytosed by cancer cells (HeLa cells) than normal cells (HEK-293 cells, i.e. Human Embryonic Kidney Cells), we incubated the fluorescein-loaded MSNP–SS–FA (25 μg mL^{-1}) with HeLa cells and HEK-293 cells in 10% fetal bovine serum (FBS) contained DMEM medium for 1 hour and 4 hours. The nuclei of both HeLa cells and HEK-293 cells were stained with 4′,6-diamino-2-phenylindole (DAPI) and monitored using a confocal laser scanning microscope (CLSM). Both HeLa cells and HEK-293 cells were shown to have green fluorescent nanoparticles in the cytoplasm as shown in Figure 7 and S9, revealing that the MSNP–SS–FA nanoparticles were endocytosed by cells. Interestingly, we observed more intracellular distribution of nanoparticles in HeLa cells than HEK-293 cells as shown in Figure 7. Thus, effective internalization of MSNP–SS–FA nanoparticles by HeLa cells indicates that the functionalization with folic acid certainly influences the uptake of MSNP–SS–FA by cancer cells, and the overexpressed folic acid receptors are involved in the cellular uptake. The next crucial step was to evaluate triggered drug delivering capability in cancer cells. Since a relatively high concentration of GSH is present in a variety of cancers, drug-loaded MSNP–SS–FA is designed

Journal of Materials Chemistry B Accepted Manuscript

to release the drug in cells triggered by the GSH-induced disulfide bond cleavage. To this end, HeLa cells incubated with Dox loaded MSNP–SS–FA at 37 ^{o}C for 2 h were investigated by confocal microscope for intracellular drug delivery. Using Dox has two advantages; it works both as an anti-cancer drug and a fluorophore. Figure 8A shows internalization of nanoparticles followed by efficient delivery of Dox in HeLa cells after 4 h of incubation. In order to test the robustness of MSNP–SS–FA, it would be necessary to further study the fate of cells after administering the drug. HeLa cells incubated with Dox loaded nanoparticles for 6 h showed distorted cells, clearly indicating drug induced apoptosis as shown in Figure 8B. The designed MSNP–SS–FA is an effective stimuli responsive drug delivery system specifically in cancer cells and overcomes the problem of enhanced cytotoxicity of Dox in normal cells due to non-target specificity.

4. Conclusions

In summary, we have designed a cancer targeted, redox responsive, Pd (II) templated rotaxane nanovalve capped mesoporous silica nanoparticle based drug delivery system. While mesoporous nanoparticles function as carriers, rotaxane nanovalve acts as the gatekeeper. Cancer cell targeting is achieved by folic acid terminals. Reducing agents such as DTT/GSH trigger the disulfide bond cleavage in MSNP–SS–FA and lead to drug delivery. No premature release in the absence of trigger molecules proves that the delivery mechanism of our designed nanoparticles is effective. This design of folic acid targeting combined with GSH triggered delivery, cleverly prevents severe side effects due to the nonspecific release of the drug. High viability of cells in the presence of these nanoparticles solves the problem of biocompatibility. Elevated levels of apoptosis in drug loaded, nanoparticle treated HeLa cells, compared to an equivalent amount of free drug

Journal of Materials Chemistry B Accepted Manuscript

clearly suggests that this design is a suitable alternative to transport and delivery of drugs in an extremely safe and effective manner.

Acknowledgements

We gratefully acknowledge the financial support of Ministry of Science and Technology (Taiwan) for supporting this research under the grant (101-2113-M-009-016-MY2) and National Chiao Tung University.

Notes and references

National Chiao Tung University, Department of Applied Chemistry, Science Building 2, 1001 Ta Hsueh Road, Hsinchu, Taiwan 300, ROC.

Associate Professor Shu-Pao Wu. TEL: 886-3-5712121 ext 56506. FAX: 886-3-5723764. E-mail: spwu@mail.nctu.edu.tw

Electronic Supplementary Information (ESI) available: Synthesis and characterization of the functional molecules and MSNPs is available in the supporting information. See DOI: 10.1039/b000000x/

1 I. I. Slowing, J. L. Vivero-Escoto, C.-W. Wu, V. S. Y. Lin, *Adv. Drug Deliv. Rev.*, 2008, **60**, 1278-1288.

2 R. W. Johnstone, A. A. Ruefli, S. W. Lowe, *Cell,* 2002, **108**, 153-164.

3 I. Brigger, C. Dubernet, P. Couvreur, *Adv. Drug Deliv. Rev.*, 2002, **54**, 631-651.

Journal of Materials Chemistry B Accepted Manuscript

4 N.-T. Chen, S.-H. Cheng, J. S. Souris, C.-T. Chen, C.-Y. Mou and L.-W. Lo, *J. Mater. Chem.*, 2013, **1**, 3128-3135.

5 M. Manzano and M. Vallet-Regi, *J. Mater. Chem.*, 2010, **20**, 5593-5604.

6 C. T. Kresge, M. E. Leonowicz, W. J. Roth, J. C. Vartuli, J. S. Beck, *Nature*, 1992, **359**,710-712.

7 I. I. Slowing, J. L. Vivero-Escoto, B. G. Trewyn and V. S. Y. Lin, *J. Mater. Chem.*, 2010, **20**, 7924-7937.

8 D. Radu, C.-Y. Lai, J. Huang, X. Shu, V. Lin, *Chem. commun.*, 2005, 1264-1266.

9 N. Gartmann, D. Bruhwiler, *Angew. Chem. Int. Ed.*, 2009, **48**, 6354-6356.

10 K. Johann, S. Axel, B. Thomas, *Chem. Mater.*, 2008, **20**, 7207-7214.

11 M. Vallet-Regi, A. Rámila, R. P. d. Real, J. Pérez-Pariente, *Chem. Mater.*, 2001, **13**, 308-311.

12 M. Vallet-Regí, *Chem. Eur. J.*, 2006, **12**, 5934-5943.

13 J. Lu, M. Liong, Z. Li, J. Zink, F. Tamanoi, *Small*, 2010, **6**, 1794-1805.

14 S. Angelos, E. Choi, F. Vogtle, L. DeCola, J. I. Zink, *J. Phys. Chem. C*, 2007, **11**, 6589-6592.

15 A. Schlossbauer, C. Dohmen, D. Schaffert, E. Wagner, T. Bein, *Angew. Chem. Int. Ed.*, 2011, **50**, 6828-6830.

16 M. K. Niveen, T. Ali, A. L. Yuen, W. A. Michael, C. F. Douglas, A. K. Hussam, I. Z. Jeffrey, J. F. Stoddart, *Eur. J. Org. Chem.*, 2009, **2009**, 1669–1673.

17 Z. Luo, K. Cai, Y. Hu, L. Zhao, P. Liu, L. Duan, W. Yang, *Angew. Chem. Int. Ed.*, 2011, **50**, 640-643.

Journal of Materials Chemistry B Accepted Manuscript

18 X. Ma, K. T. Nguyen, P. Borah, C. Y. Ang, Y. Zhao, *Adv. Healthcare Mater.*, 2012, **1**, 690-697.

19 N. Mal, M. Fujiwara, Y. Tanaka, *Nature*, 2003, **421**, 350-353.

20 L. Zhao, J. Peng, Q. Huang, C. Li, M. Chen, Y. Sun, Q. Lin, L. Zhu, F. Li, *Adv. Funct. Mater.*, 2014, **24**, 363-371.

21 J. Geng, M. Li, L. Wu, C. Chen, X. Qu, *Adv. Healthcare Mater.*, 2012, **1**, 332-336.

22 F. Porta, G. E. Lamers, J. Morrhayim, A. Chatzopoulou, M. Schaaf, H. den Dulk, C. Backendorf, J. I. Zink, A. Kros, *Adv. Healthcare Mater.*, 2013, **2**, 281-286.

23 A. Schlossbauer, J. Kecht, T. Bein, *Angew. Chem. Int. Ed.*, 2009, **48**, 3092-3095.

24 Y. Lin, C. Tsai, H. Huang, C. Kuo, Y. Hung. D. Huang, Y. Chen, C. Mou, *Chem. Mater.*, 2005, **17**, 4570-4573.

25 I. Slowing, B. Trewyn, V. Lin, *J. Am. Chem. Soc.*, 2006, **128**, 14792-14793.

26 D. Tarn, C. Ashley, M. Xue, E. Carnes, J. Zink, C. Brinker, *Acc. Chem. Res.*, 2013, **46**, 792–801.

27 T. Xia, M. Kovochich, M. Liong, H. Meng, S. Kabehie, S. George, J. Zink, A. Nel, *ACS nano*, 2009, **3**, 3273-3286.

28 A. Jemal, F. Bray, M. Center, J. Ferlay, E. Ward, D. Forman, *CA: a cancer journal for clinicians*, 2011, **61**, 69-90.

29 T. Daniels, T. Delgado, G. Helguera, M. Penichet, *Clin. immunol.*, 2006, **121**, 159-176.

30 J. Zhang, Z. F. Yuan, Y. Wang, W. H. Chen, G. F. Luo, S. X. Cheng, R. X. Zhuo, X. Z. Zhang, *J. Am. Chem. Soc.*, 2013, **135**, 5068-5073.

31 M. Xie, H. Shi, Z. Li, H. Shen, K. Ma, B. Li, S. Shen, Y. Jin, *Colloids Surf. B*, 2013 **110**, 138-147.

Journal of Materials Chemistry B Accepted Manuscript

32 G. K. Balendiran, R. Dabur, D. Fraser, *Cell Biochem. Funct.*, 2004, **22**, 343-352.

33 S. Chia, J. Cao, J. F. Stoddart, J. I. Zink, *Angew. Chem. Int. Ed.*, 2001, **113**, 2513-2517.

34 T. D. Nguyen, H.-R. Tseng, P. C. Celestre, A. H. Flood, Y. Liu, J. F. Stoddart, J. I. Zink, *Proc. Natl. Acad. Sci. U.S.A.*, 2005, **102**, 10029-10034.

35 Z. Li, J. C. Barnes, A. Bosoy, J. F. Stoddart, J. I. Zink, *Chem. Soc. Rev.*, 2012, **41**, 2590-2605.

36 C. O. Dietrich-Buchecker, J.-P. Kintzinger and J.-P. Sauvage, *Tetrahedron Lett.*, 1983, **24**, 5095-5098.

37 C. F. Meares, T. G. Wensel, *Acc. Chem. Res.*, 1984, **17**, 202-209.

38 H. B. Gray, *Proc. Natl. Acad. Sci. U.S.A.*, 2003, **100**, 3563-3568.

39 M. A. Hanif, I. I. Ebralidze, J. H. Horton, *Appl. Surf. Sci.*, 2013, **280**, 836-844.

Journal of Materials Chemistry B Accepted Manuscript

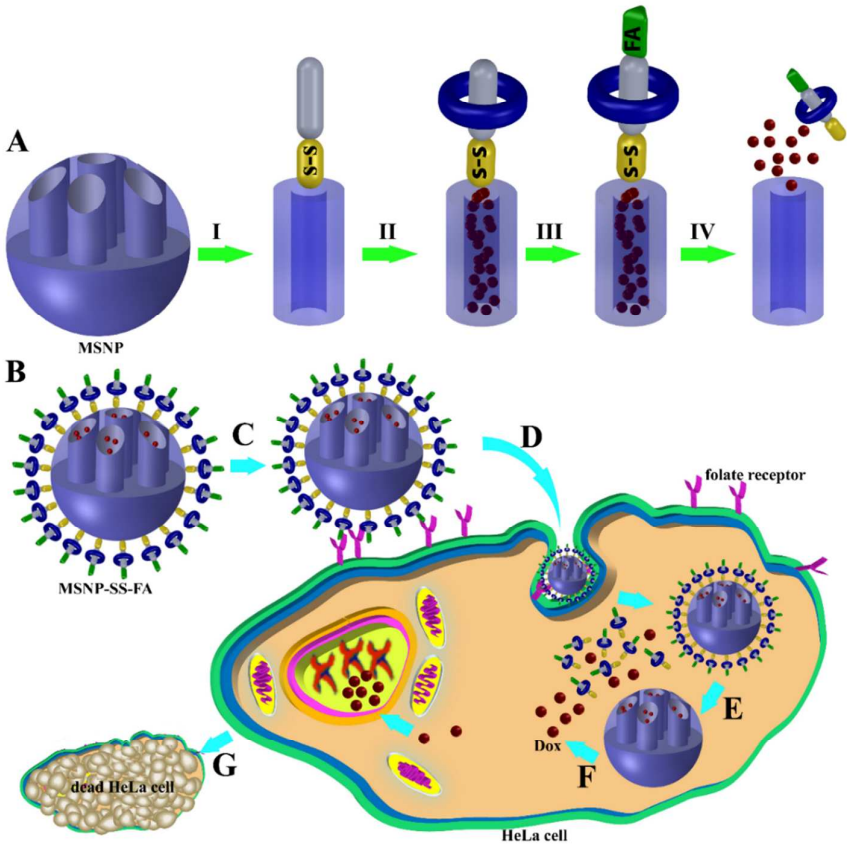

Figure 1. (A) Functionalization protocol of MSNPs, Stage I: surface functionalization of MSNPs with stalk containing disulfide bond; Stage II: Dox loading, rotaxane nanovalve capping on the surface of MSNP (MSNP–SS–N_3); stage III: folic acid functionalization on MSNP–SS–N_3; stage IV: controlled release of drug by uncapping the rotaxane nanovalve with DTT/GSH. (B) Drug loaded MSNP–SS–FA under physiological condition. (C) folic acid targeted recognition by folate receptors on cancer cell. (D) Receptor mediated endocytosis of nanoparticle in to the cancer cell. (E) glutathione-triggered drug release inside the cell. (F) Apoptosis of HeLa cells.

Journal of Materials Chemistry B Accepted Manuscript

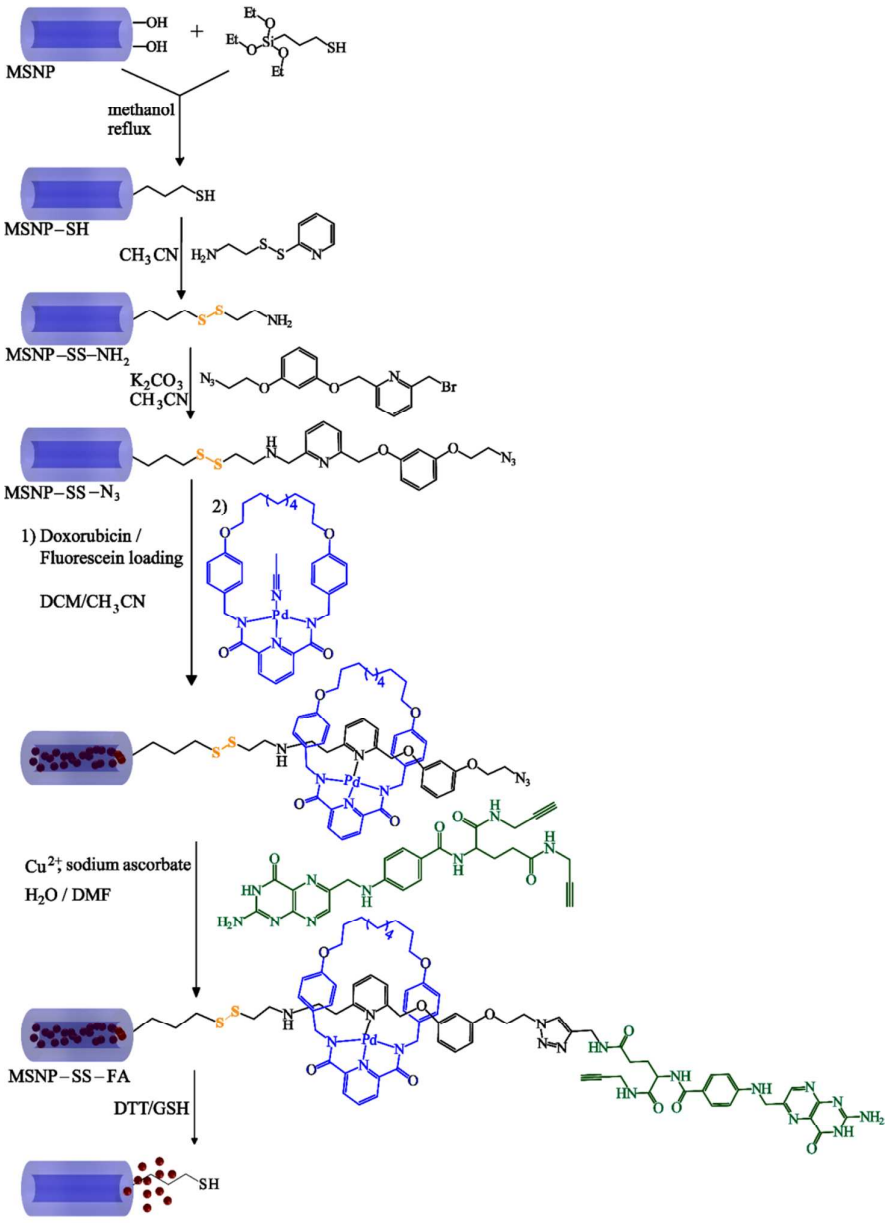

Figure 2. Synthesis of folic acid functionalized mesoporous silica nanoparticle; the nanoparticles are loaded with doxorubicin/fluorescein which is released upon the cleavage of disulfide bond by reducing agents DTT and GSH.

Journal of Materials Chemistry B Accepted Manuscript

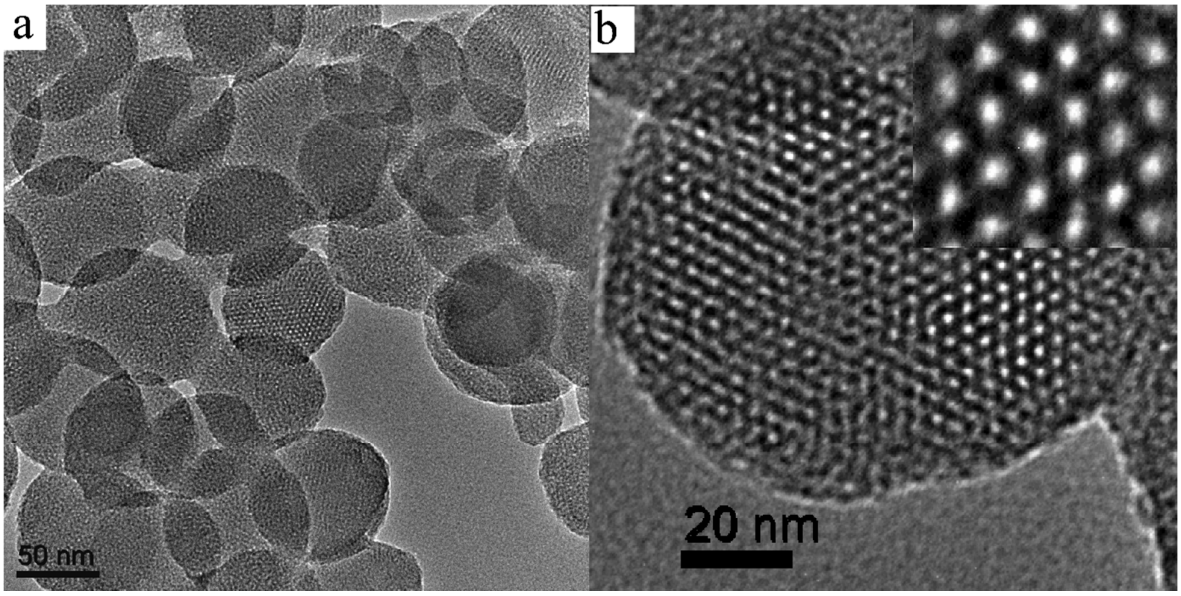

Figure 3. (a) HR-TEM and (b) enlarged HR-TEM images of **MSNP-SS-N_3**

Journal of Materials Chemistry B Accepted Manuscript

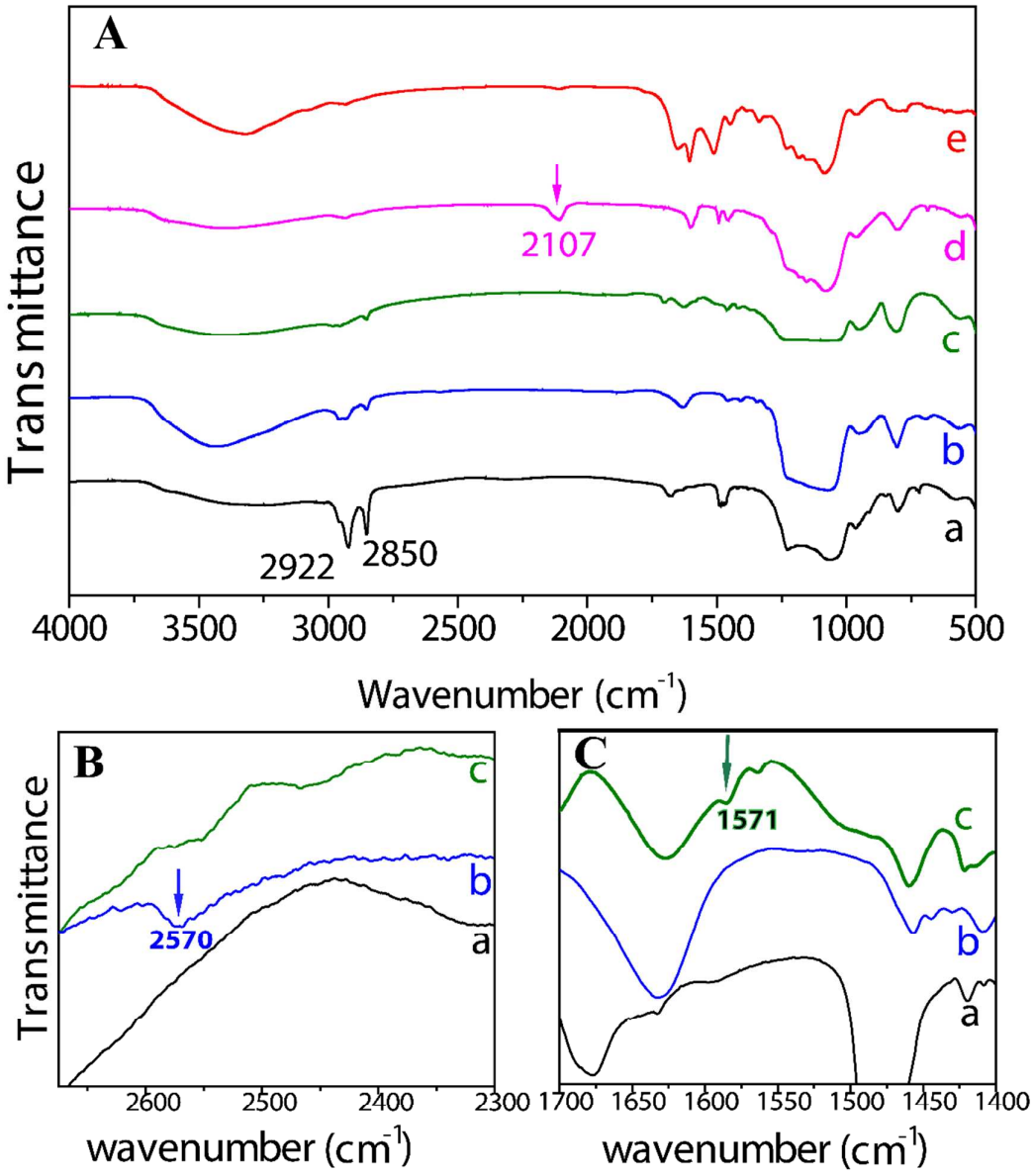

Figure 4. FT-IR spectra of silica nanoparticles under indicated conditions: (a) MSNPs containing surfactants, (b) MSNP–SH, (c) MSNP–SS–NH_2, (d) MSNP–SS–N_3, and (e) MSNP–SS–FA. (A) FT-IR spectra of silica nanoparticles, (B) and (C) are expanded FT-IR spectra of (A)

Journal of Materials Chemistry B Accepted Manuscript

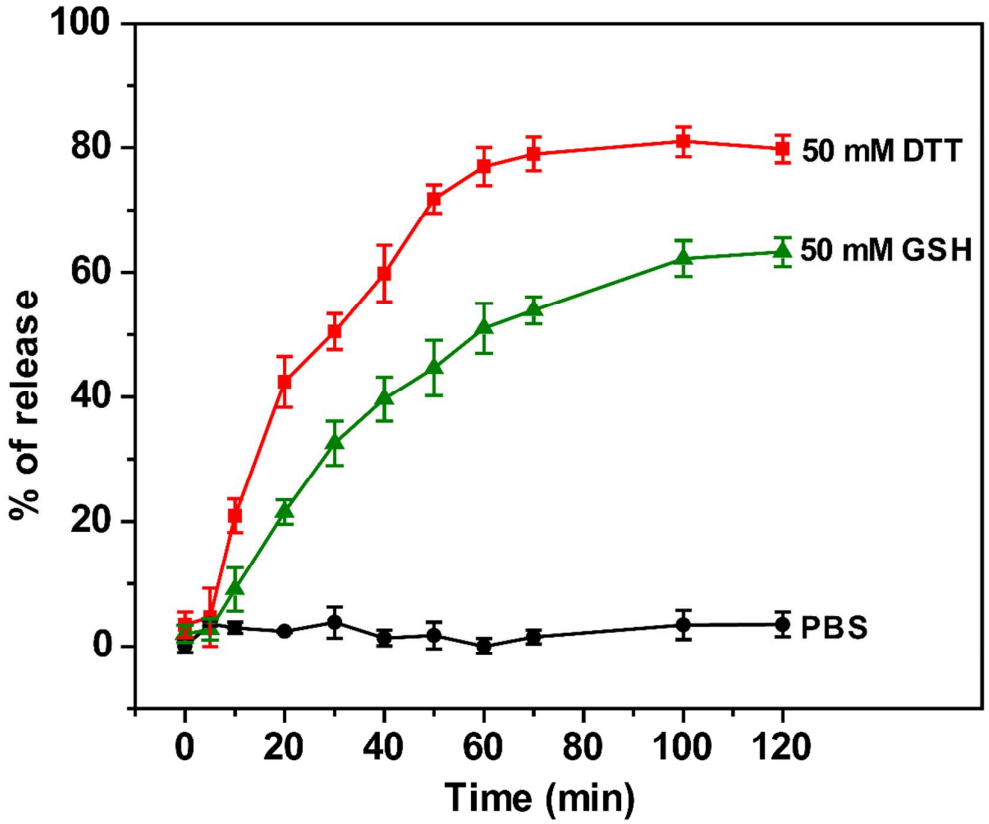

Figure 5. Controlled release of fluorescein with addition of reducing agent DTT and GSH in PBS buffer (pH = 7.4). Curve (●) indicates the release profile of fluorescein loaded MSNP–SS–FA without any reducing agent. Curve (■) and (▲) indicate the release profile of fluorescein loaded MSNP–SS–FA with addition of 50 mM of DTT and 50 mM of GSH, respectively.

Journal of Materials Chemistry B Accepted Manuscript

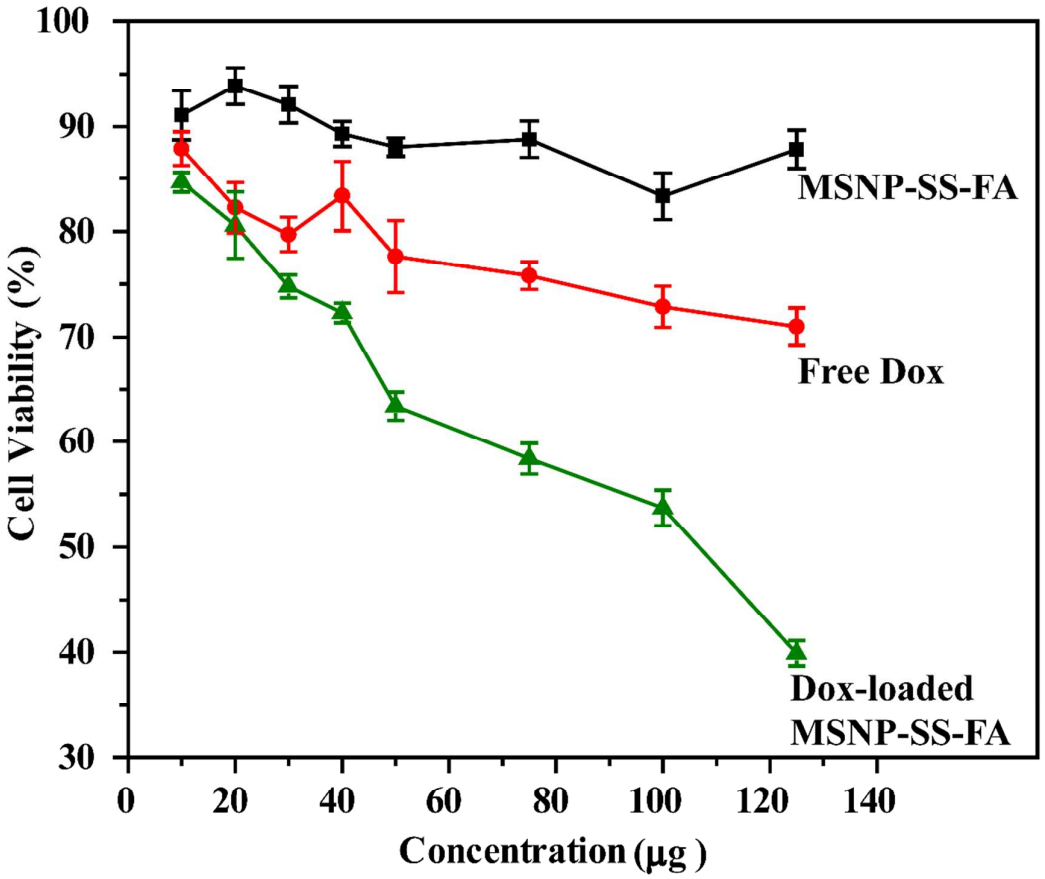

Figure 6. Viabilities of HeLa cells after being treated with indicated nanoparticles and equivalent amount of free Dox for 24 h. Curves ■,● , and▲ indicate the cell viabilities in the presence of MSNP–SS–FA, free Dox, and Dox-loaded MSNP–SS–FA respectively, under the concentrations measured.

Journal of Materials Chemistry B Accepted Manuscript

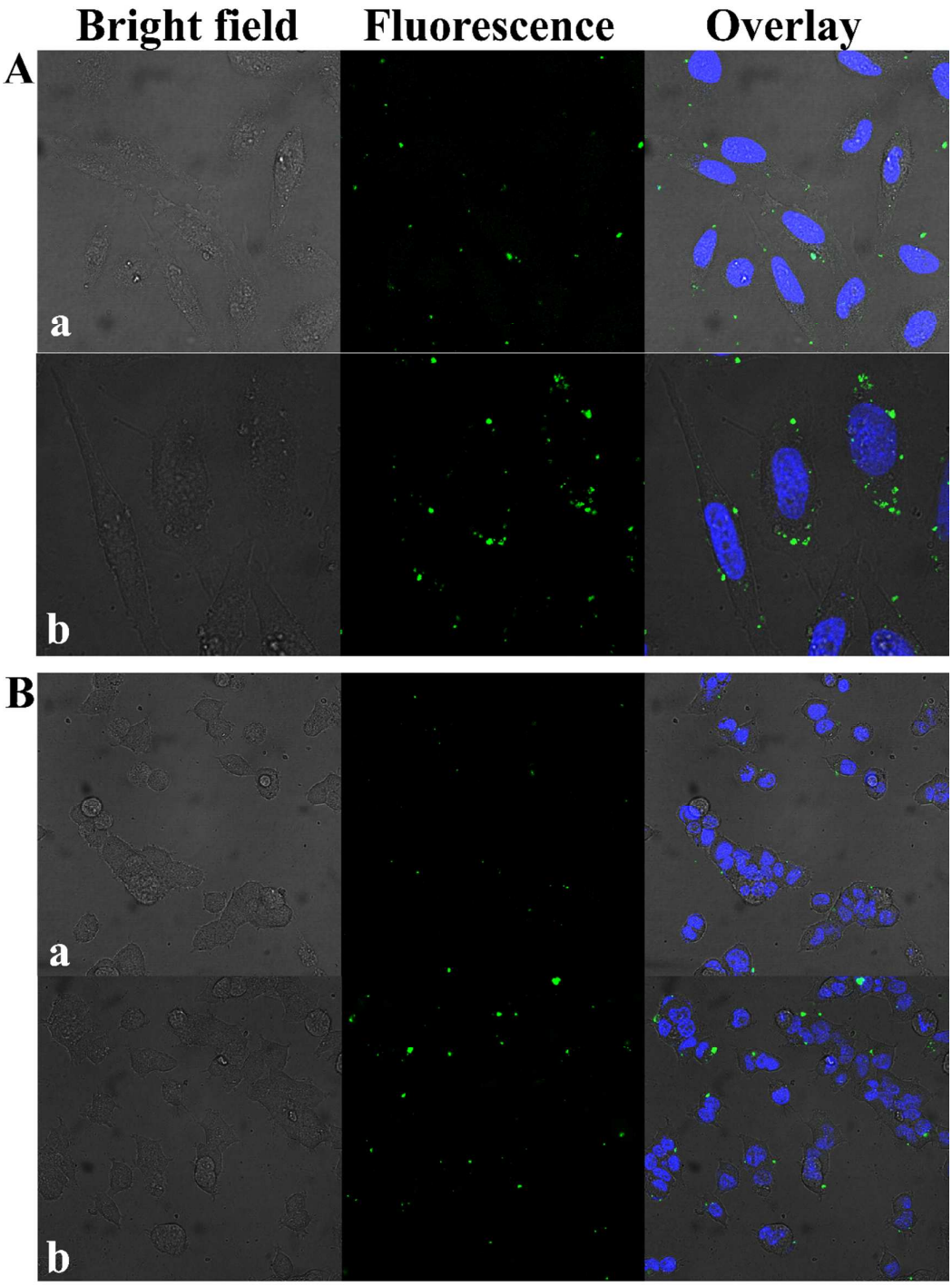

Figure 7. Fluorescence microscopic images of (A) HeLa cells and (B) HEK-293 cells after being treated with 25 μg mL^{-1} of fluorescein-loaded MSNP-SS-FA nanoparticles (a) for 1hour and (b) for 4 hours at 37 °C. Blue signal is given by nuclei and green signal is given by nanoparticles.

Journal of Materials Chemistry B Accepted Manuscript

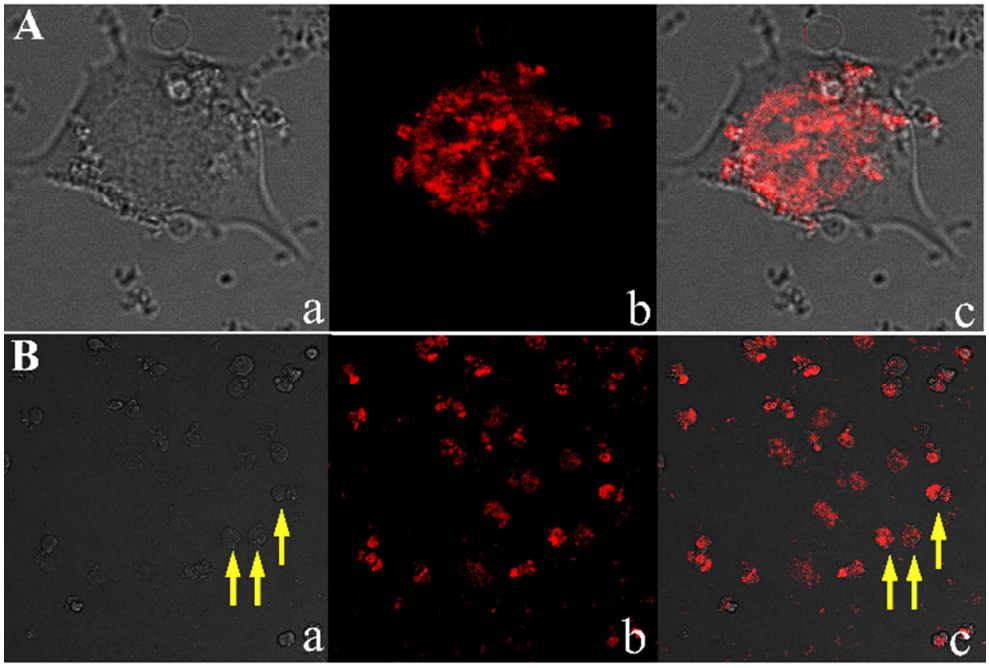

Figure 8. Fluorescence microscopic images of HeLa cells after being treated with 50 μg mL^{-1} of Dox-loaded MSNP-SS-FA. (A) after 4 h at 37 °C, (B) after 6 h at 37 °C. Yellow colored arrows shows apoptosis of HeLa cells induced by Dox.

Journal of Materials Chemistry B Accepted Manuscript

Redox Responsive Pd (II) Templated Rotaxane Nanovalve Capped Mesoporous Silica Nanoparticles: A Folic Acid Mediated Biocompatible Cancer-targeted Drug Delivery System

Srivardhan Reddy Gayam, Shu–Pao Wu*

Department of Applied Chemistry, National Chiao Tung University, Hsinchu, 30010, Taiwan, Republic of China

Herein, redox responsive Pd (II) templated rotaxane nanovalve capped mesoporous silica nanoparticles were designed for effective cancer-targeted drug delivering system.

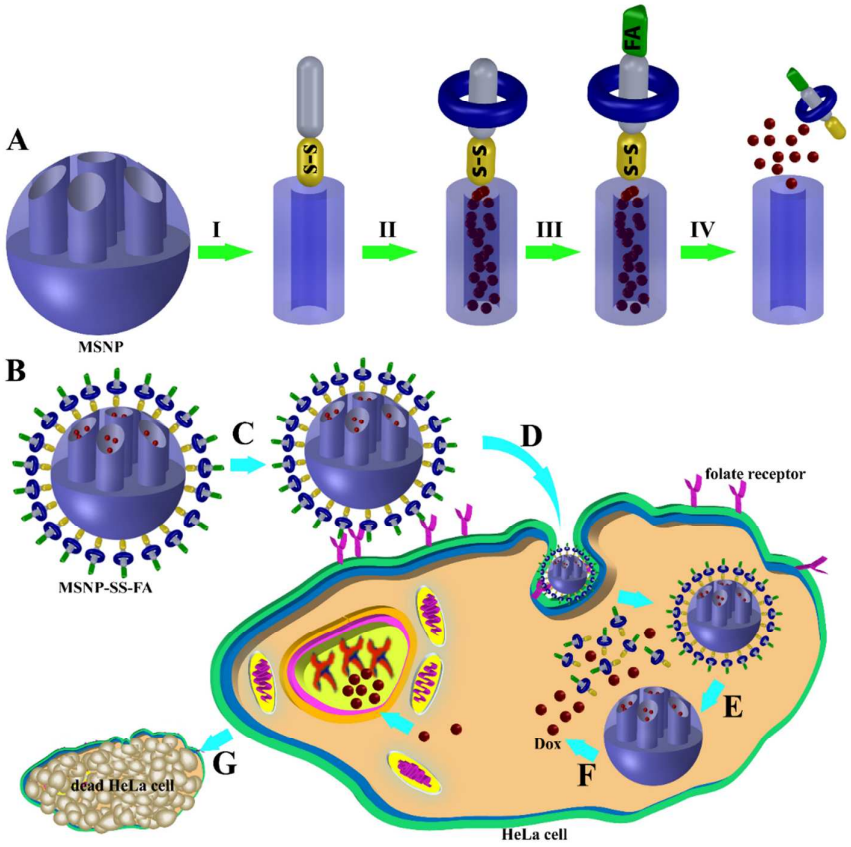

Journal of Materials Chemistry B Accepted Manuscript